Effect of Duxseal on horizontal stress and soil stiffness in small-amplitude dynamic centrifuge models

Ge Cui[1]*, Charles Heron[1], and Alec Marshall[1]

ABSTRACT

The constitutive behavior of soil is stress dependent. Therefore, geotechnical centrifuges are widely used to replicate full-scale stress fields, thereby ensuring the correct soil response within reduced-scale centrifuge models. A vibration absorbing material (such as Duxseal) is commonly employed to reduce the effect of reflected waves generated at the boundaries of rigid containers in dynamic centrifuge tests. However, such a material has the potential to deform laterally under the high horizontal stresses applied within centrifuge tests and consequently the initial at rest lateral earth pressure condition will not be maintained. A procedure to back-calculate the lateral earth pressure coefficient (K) is presented in this paper. In addition, two experimental methods, which are implemented to evaluate K by measuring the shear wave velocity from centrifuge-based air hammer testing and triaxial based bender element testing, are described. Results demonstrate that significant lateral earth pressure and soil stiffness reductions are observed within the upper soil region (top third of the model depth). In addition, the appropriate manipulation of the cross-correlation method used to process shear wave signals is discussed and an empirical equation to predict the small strain shear modulus of the dry silica sand (HST95 Congleton sand) used in this study is provided. Outcomes of this study are directly applicable to small-amplitude dynamic centrifuge tests such as ground-borne vibrations; some factors relating to large-amplitude seismic studies, such as soil inertial effects and

1 Department of Civil Engineering, University of Nottingham, Nottinghamshire, NG7 2RD, UK.

* Corresponding author, E-mail: ezzgc2@nottingham.ac.uk.

Charles Heron, E-mail: ezzcmh@nottingham.ac.uk.

Alec Marshall, E-mail: evzamm@nottingham.ac.uk.

higher shear strains, are not considered.

Keywords

dynamic centrifuge test, boundary condition, Duxseal, shear wave velocity, lateral earth pressure coefficient

1 Introduction

Ground-borne dynamic events can be generated in a variety of ways, including natural disasters, such as earthquakes and volcanic eruptions, and human actions, such as construction activities, the operation of heavy trucks, and underground railways. Numerous studies have been undertaken using geotechnical centrifuges to investigate these different dynamic scenarios (Zeng and Schofield 1996; Coelho et al. 2003; Yang et al. 2013a, 2013b). When creating small-scale geotechnical centrifuge models, it is important to replicate the stress profile of the full-scale scenario. To achieve the correct initial at-rest lateral earth pressure (K_0), model containers with rigid walls are employed to maintain a zero lateral strain condition (initial K_0 condition) (Zeng and Schofield 1996). In the idealized prototype scenario, soil layers are 'infinitely wide' and hence any generated vibrations propagate within an infinite soil layer. However, centrifuge models must be enclosed within a container with finite boundaries, which can lead to boundary effects. One common issue caused by rigid boundaries is that dynamic waves reflect back into the soil layer, contrary to the idealized prototype full-scale scenario being modelled. At some frequencies, the incident and reflected waves will be in phase and will amplify the soil response (known as constructive interference). To the contrary, destructive interference can appear at other frequencies if waves are out of phase, which leads to a decrease of soil response.

To minimize the boundary effects, a material capable of absorbing incident waves is placed around the inside surface of the rigid containers. This reduces the magnitude of reflections and hence replicates the idealized prototype scenario more accurately (Zeng and Schofield, 1996). Conventional absorbing materials used by centrifuge modelers have included foam (Ha et al. 2011), sponge rubber (Itoh et al. 2005) and Duxseal (Madabhushi 1991; Pak and Guzina 1995; Cheney et al. 1990; Yang et al. 2013a, 2013b; Cilingir 2009). However, the effectiveness of certain materials, for example foam and sponge rubber, have not been carefully investigated (Yang 2012).

Duxseal (an oil based industrial fill material) is a multi-purpose sealing and caulking rubber compound with adhesion and shape retention properties. It has a heavy, putty-like consistency and will remain pliable and useable even when exposed to air over a long period of time. It was found by Madabhushi (1991) that Duxseal can absorb approximately 65% of incident P-waves and 60% of incident S-waves. As a result, Duxseal has been widely used in recent decades for dynamic centrifuge testing to investigate a wide variety of problems. It is particularly useful within experiments employing the use of a transparent side window for image analysis which require rigid boundaries (instead of a laminar box) (Chian and Madabhushi 2013; Chian et al. 2014; Heron et al. 2015; Adamidis and Madabhushi 2018; Kassas et al. 2020; Madabhushi and Haigh 2021; Kassas et al. 2021; Adamidis and Madabhushi 2021).

Dynamic centrifuge tests employing Duxseal or other energy-absorbing materials along their boundaries mainly consist of two categories: earthquake induced events with relatively large ground movement amplitudes and ground-borne vibration problems with small amplitude ground movements. The majority of these studies focus on the former category and relate to free-field ground motions (Pak et al. 2011; Soudkhah and Pak 2012; Zhu et al. 2018), retaining wall behavior (Dewoolkar et al. 2001; Madabhushi and Haigh 2019; Madabhushi and Haigh 2021), shallow foundations (Chakrabortty and Popescu 2012; Heron et al. 2015; Adamidis and Madabhushi 2018; Kassas et al. 2020; Kassas et al. 2021; Adamidis and Madabhushi 2021), basement structures sited on liquefiable soil (Hughes and Madabhushi 2018), and underground structures (Cilingir and Madabhushi 2011; Chian and Madabhushi 2013; Chian et al. 2014). The latter category has mainly related to railway induced ground-borne vibrations and soil-structure interactions, including vibrations from surface (Yang et al. 2013b) and underground railways (Yang et al. 2013a). It should be noted that ground-borne vibration related problems have gained more attention in recent years due to increasingly stringent requirements for infrastructure development projects to eliminate/limit effects on nearby homes and businesses.

Despite its advantages, Duxseal and other energy absorbing materials can cause unwanted issues. As highlighted by Zeng and Schofield (1996), the strength and stiffness of Duxseal is difficult to determine in standard laboratory tests and, because of the lack of reliable strength and stiffness parameters, there is a corresponding lack of numerical analysis studying its impact on overall model behavior. One of the key impacts, but as yet unstudied, of including Duxseal is its effect on the lateral stiffness of the boundary and hence upon the K_0 and soil stiffness conditions. Pak and Guzina (1995) discussed how the compressibility of Duxseal can lead to unrealistic deformations, causing small failure wedges around the side of the soil model. Ultimately, there is a trade-off between the advantages of Duxseal (or other energy absorbing materials) to reduce boundary reflections and the issues it causes in relation to soil stiffness and stress profiles. Currently, however, there is a lack of studies which allow centrifuge modelers to quantify the adverse effects of Duxseal.

Recent research at the University of Nottingham Centre for Geomechanics (NCG) studied railway induced ground-borne vibrations (GBV) using a geotechnical centrifuge. Tests were conducted which focused on the vertical oscillation of a single pile embedded within a dry silica sand (Congleton sand) and the resulting GBV (Cui et al. 2018). Duxseal was used to reduce wave reflections from the rigid boundaries of a circular container. Prior to the GBV study, a comprehensive investigation into the impact of Duxseal, with an emphasis on the lateral stiffness of the boundary and hence the effect on the soil stress profile and soil stiffness conditions, was undertaken using an indirect method to evaluate the lateral earth pressure coefficient within a centrifuge model: an empirical equation was derived to back-calculate the lateral earth pressure coefficient from measured shear wave velocity values. This indirect method involves combining results from two shear wave velocity measurement methods: air hammer testing in the centrifuge and bender element testing in a triaxial cell. This paper presents the results from these two methods and uses the results to quantify the lateral deformation induced impact on lateral earth pressure and soil stiffness, by the inclusion of Duxseal. Additionally, nuances in the data processing methods used to obtain the shear wave velocity, which has not been discussed by previous researchers, are detailed in this study. The main focus of this paper is to demonstrate and quantify (for a specific case) the effect of an energy-absorbing boundary on the initial stress field and small strain shear modulus of a centrifuge model. Outcomes should motivate the geotechnical physical modelling community to consider the potential effects of the use of vibration absorbing materials on their dynamic physical models.

2 Small Strain Shear Modulus

Soil behavior is non-linear; the magnitude of strain experienced by the soil impacts various important mechanical properties of the soil. The shear strain levels were classified by Ishihara (1996) into four ranges: small, medium, large, and failure. Within the small shear strain level, less than 10^{-5}, the assumption of linear elastic soil behavior is appropriate (Kouroussis et al. 2014; Lombaert et al. 2015; BS 2005). Consequently, the small-strain shear modulus (G_{max}) is a commonly quoted and adopted parameter in geotechnical analysis (Rollins et al. 1998). G_{max} can be estimated as

$$G_{max} = \rho v_s^2 \tag{1}$$

using a measured shear wave velocity v_s and soil density ρ.

The shear wave velocity can be measured by determining the shear wave travel time between two transducers spaced at a known distance. Several methods have been developed by centrifuge modelers to generate shear waves in-flight, including the use of bender elements (Brandenberg et al. 2006; Lee et al. 2012; Kim 2010; Lee et al. 2014) and air-hammers (Ghosh and Madabhushi 2002; Arulnathan et al. 2000). Both methods can provide shear waves that are large enough to be detected by standard transducers yet sufficiently small such that the induced shear strain magnitude remains within the small strain range (allowing the use of Equation 1). Because the shear wave detector transducers (accelerometers) are embedded in the soil model at discrete locations, experimental measurements in the centrifuge only measure v_s as an average over the region between transducers, for example across a certain soil depth.

Shear wave velocity can also be measured in the laboratory at the element scale using triaxial based bender element (BE) tests. In a triaxial test, the principal stresses within the soil sample can be controlled and measured precisely and hence a more reliable variation of shear wave velocity, and hence stiffness, with confining stress can be ascertained. It should be noted that this assumes the stress state within the triaxial soil sample is uniform. By contrast, there is no commonly available method to accurately and unobtrusively measure the in-situ horizontal stresses within a centrifuge model.

3 Experimental Measurement of Shear Wave Velocity

In this study, both air hammer and bender element testing were used to measure the shear wave velocity, with the combined results used to understand the effect of Duxseal. The air hammer testing in the centrifuge was used to provide an average shear wave velocity over a soil layer, whereas the bender element testing in a triaxial cell was used to establish an empirical equation (a function of lateral earth pressure coefficient K) which predicts the mean shear wave velocity of a soil layer. The combined results enable back-calculation of the lateral earth pressure coefficient of a soil layer. By conducting air hammer tests with and without the presence of Duxseal, the impact of Duxseal on the lateral earth pressure coefficient and the soil stiffness was quantified. The two experimental methods used in this study are presented in this section.

3.1 Model soil and sample preparation

Dry HST95 Congleton sand (a very fine and uniformly rounded silica sand) was used in this study to conduct all tests. The basic parameters of the Congleton sand are shown in Table 1 (Lauder 2010). The dry Congleton sand was air pluviated using a flow rate and drop height calibrated to obtain a relative density of approximately 85% during the preparation of the centrifuge models and the bender element triaxial samples. Repeated calibration tests were conducted to ensure the variability of relative density of the soil was within +/- 2% of the stated relative density.

TABLE 1 Physical properties of HST95 silica Congleton sand (Lauder 2010)

Parameter	Value	Parameter	Value
Specific gravity (G_s)	2.63	Minimum dry unit weight ($\gamma_{d,min}$)	14.6 kN/m^3
D_{10}	0.10 mm	Maximum dry unit weigh ($\gamma_{d,max}$)	17.6 kN/m^3
D_{30}	0.12 mm	Minimum void ratio (e_{min})	0.467
D_{50}	0.13 mm	Maximum void ratio (e_{max})	0.769
D_{60}	0.14 mm	Critical state friction angle (φ')	31°

3.2 Air hammer test in the centrifuge

A miniature air hammer (AHA), see FIG. 1, was used in the centrifuge to generate shear waves. The air hammer is a 110 mm long tube with a thin layer of Congleton sand glued to the outer surface to ensure shear waves are effectively transferred to the surrounding soil. The air hammer tube consists of a brass tube, two stainless steel couplers and two stainless steel push-fit adaptors, as shown in FIG. 1. To generate shear waves within the soil, air is supplied from one end of the tube, and a 20 mm long pellet inside the tube is forced to impact the other end of the tube. The pellet is made of two PTFE hollow cylinders, one stainless steel cylinder and two stainless steel bolts, as shown in FIG. 1. Therefore, a stainless steel-to-stainless steel contact is made when the pellet hits the air hammer tube. Consequently, the tube moves slightly in the soil, generating a small shear wave, the magnitude of which can be controlled by adjusting the inlet air pressure. To detect and record shear waves, a vertical array of micro-electromechanical system (MEMS) accelerometers (labelled AHA-M in FIG. 1) was positioned above the air hammer. Four MEMS accelerometers (type: ADXL001-70BEZ) were mounted on a continual flexible plastic sheet (shown in FIG. 1) to obtain accurate inter-instrument spacing (120 mm). For this testing, it is important to ensure that a) all the MEMS accelerometers are precisely on the same vertical line, b) each MEMS accelerometer is placed at the desired location (otherwise, inter-instrument spacing and consequently travel time measurements may be inaccurate). The continuous flexible plastic sheet ensures the inter-instrument spacing is known, thus providing reliable shear wave velocity measurements, which is the most important measurement for this study. Preliminary tests were carried out to check that shear waves generated by the air hammer were well captured by these MEMS accelerometers. As the flexible plastic strip used is significantly less stiff than the surrounding soil, especially when at elevated g-level in the centrifuge, the impact of the continuous strip within the soil will be negligible.

A high sampling rate of 100 kHz was used to record the acceleration time histories to avoid low-resolution errors (Lee et al. 2014). Preliminary tests were conducted to determine the appropriate air pressure for the air hammer tests. It was found that 50 to 100 kPa was sufficient to generate the impact while minimizing the shear strain level to ensure measurements would give a good evaluation of G_{max}. The peak shear strain amplitude can be estimated from the recorded accelerations by the MEMS accelerometers using the approximation of an equivalent sinusoidal wave with an angular frequency of ω and a peak acceleration of a_0. The peak shear strain amplitude can be calculated by $\frac{a_0}{\omega v_s}$ (Arulnathan et al. 2000). Results indicated that the shear strain amplitudes generated by the air hammer varied from 5.8×10^{-6} to 1.4×10^{-5}, with the higher strains being closest to the source. The shear strains generated by the miniature air hammer were small enough to avoid nonlinear soil behavior ($<10^{-5}$), thus providing the small-strain shear modulus G_{max}.

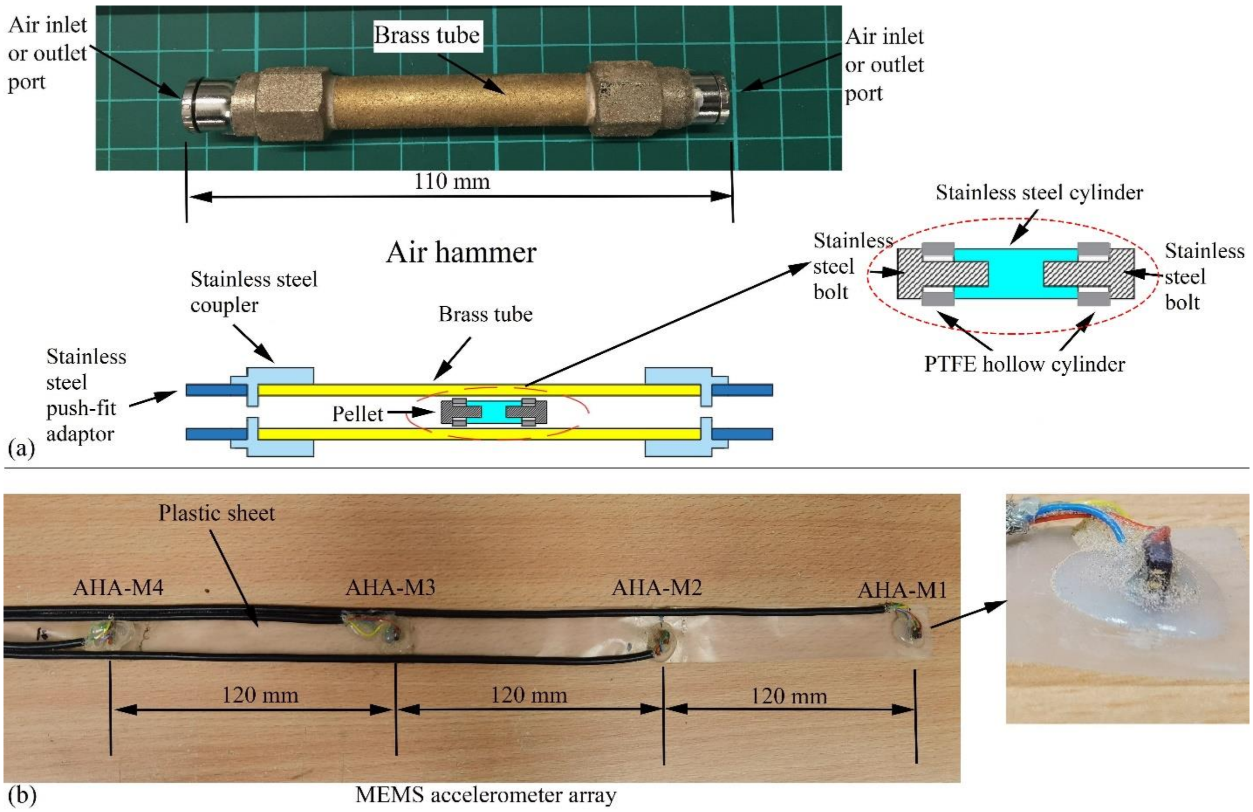

FIG. 1 (a) Air hammer (b) MEMS accelerometer array

As shown in FIG. 2, a 500 mm diameter cylindrical steel container with a depth of 500 mm was used for the centrifuge tests, which were performed at a nominal acceleration of 60 g. All centrifuge tests were carried out using the Nottingham Centre for Geomechanics (NCG) beam centrifuge at the University of Nottingham. To investigate the effect of Duxseal on the horizontal stress and soil stiffness, two air hammer (AHA) tests were carried out: AHA-T1 and AHA-T2. In AHA-T1, only the base of the model container was lined with Duxseal (34 mm thick). In AHA-T2, the entire steel container was lined with

Duxseal to a thickness of 19 mm along the walls and 34 mm on the base. Different thicknesses have been adopted by previous researchers: 25mm by Madabhushi (1991), 20 mm by Yang et al. (2013a), and 30 mm by Cilingir (2009). As mentioned in the introduction to this paper, Madabhushi (1991) found that 25 mm thick Duxseal along the side walls of a container can absorb at least 65% of incident P-waves and 60% of incident S-waves within the centrifuge. It can be assumed that a thicker Duxseal layer can absorb more incident waves, thus further reducing wave reflections form the boundary. Therefore, a thicker Duxseal layer, 34 mm, was used for the model container base, attempting to eliminate the effect of p-wave reflections emanating from the base of a pile which was being vertically vibrated within the soil layer. A thickness of 19 mm was adopted for the side walls to investigate the effects of Duxseal on the model soil stress and stiffness profiles. The four MEMS accelerometers (AHA-M1, AHA-M2, AHA-M3 and AHA-M4) were installed, as shown in FIG. 2, to measure the average shear wave velocities ($v_{s,.AHA,1}$, $v_{s,AHA,2}$ and $v_{s,AHA,3}$) of three soil layers (L_1, L_2 and L_3).

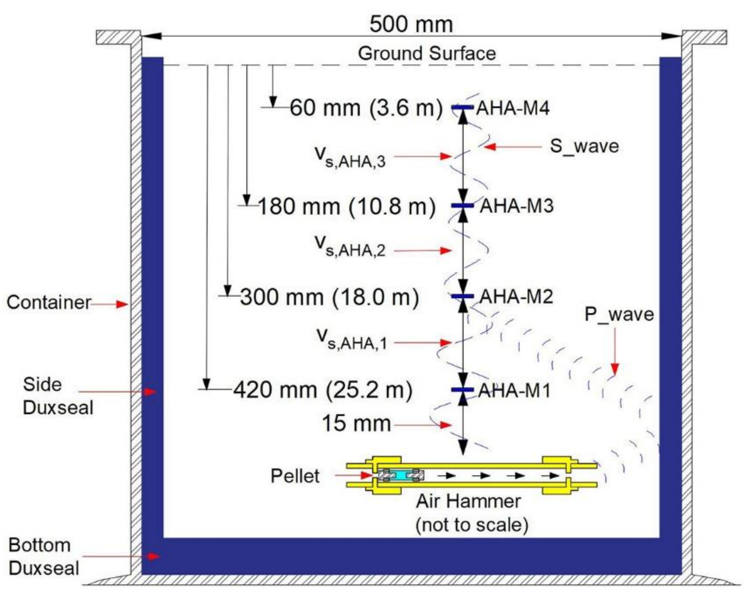

FIG. 2 Air hammer test setup (prototype scale depths shown in brackets)

3.3 Triaxial bender element tests

Bender element tests were conducted to obtain an empirical method for estimating the mean shear wave velocity of a soil layer. To obtain this empirical solution, a series of bender element tests were carried out to obtain a method for predicting the shear wave velocity at a certain depth (under a certain confining stress), which is detailed in this section. The empirical solution to estimate the mean shear wave velocity over a layer of soil is derived in Section 4.

3.3.1 Empirical estimate of shear wave velocity

In addition to experimental methods, empirical equations have been developed by researchers to predict G_{max}. There are various factors that affect the magnitude of G_{max}, including mean effective stress (confining stress), void ratio, geologic age, particle properties, and over-consolidation ratio (Dobry and Vucetic 1987; El-Sekelly et al. 2014). This study focused solely on the effect of confining stress and hence held all other influencing parameters constant. The following equation, proposed by Hardin and Richart (1963), predicts G_{max} of normally deposited dry sands.

$$G_{max} = B\frac{(a-e)^2}{1+e}(\sigma_m')^n \tag{2}$$

where e is the void ratio of the soil, σ_m' is the mean effective stress (in kPa), and B,a and n are constants.

The constants B and a depend on the grain shape and the grain-size distribution. The constants a and n can be taken as 2.17 and 0.5, respectively, for dry sands according to the results obtained by Hardin and Richart (1963). Previous research done by Cui et al. (2018) compared measured values with results using Equation 2 and confirmed that these constants can be used to provide reliable estimates for the sand adopted in the current study. Stokoe et al. (1985) found that, for shear waves travelling vertically in dry soil, the vertical and horizontal effective stresses, σ_v' and σ_h', contribute equally to G_{max}, and showed that the mean effective stress σ_m' in Equation 2 could be taken as:

$$\sigma_m' = (\sigma_v')^{0.5}(\sigma_h')^{0.5} = (\sigma_v')^{0.5}(K\sigma_v')^{0.5} = (\sigma_v')(K)^{0.5} \tag{3}$$

Therefore, Equations 1-3 can be manipulated to obtain the following expression for v_s under a certain confining pressure:

$$v_s = \sqrt{B\frac{(2.17-e)^2}{(1+e)\rho(\sigma_v')^{0.5}(K)^{0.25}}} \tag{4}$$

The constant B varies with the sand type, due to differences in particle shape and the particle size distribution. The constant B can be determined by analyzing the results from triaxial based bender element tests, as discussed in the following section.

3.3.2 Bender element testing

In this study, the GDS Bender Element System (GDS-BES) was used to measure wave velocities in a triaxial cell and to ascertain the constant B in Equation 4. As shown in FIG. 3, two bender elements with a tip-to-tip distance L_{TT} were mounted in a triaxial cell top cap and pedestal and embedded within dry soil specimens with a diameter D=50 mm and height H=100 mm. A sine wave signal was used throughout this study to perform bender element testing and a high sampling rate of 2000 kHz was adopted to obtain high resolution calculations of wave velocities.

Eleven different confining stress values corresponding to eleven depths within the centrifuge model (3.6 to 21.6 m with an interval of 1.8 m; at prototype scale) were selected based on the embedded depths of the MEMS accelerometers used for the air hammer testing within the centrifuge (see FIG. 2). Two stress states, anisotropic with K=0.5 and isotropic (K=1.0), were used to: a) provide sufficient data to obtain a reliable value for constant B, and b) verify that the constant B is stress state independent.

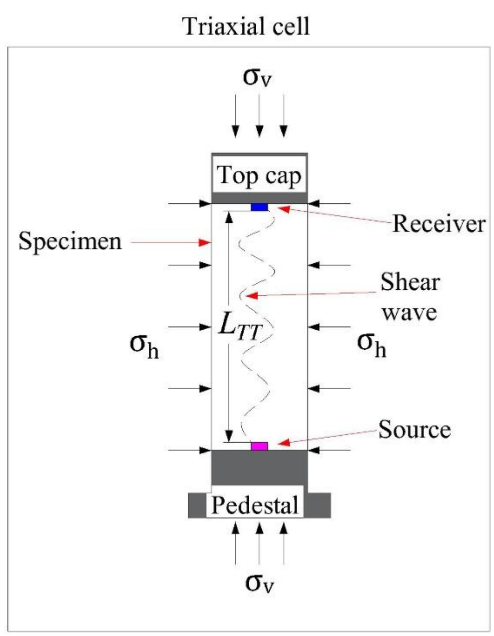

FIG. 3 A schematic view of the bender element testing in a triaxial cell

4 Quantification of the impact of lateral strain on stress condition in the centrifuge

Determination and examination of the lateral earth pressure coefficient provides a means of quantifying the impact of any lateral strain induced by the presence of Duxseal. The lateral earth pressure coefficient can be determined from the results of the bender element and air hammer tests. Firstly, the bender element test results are used to develop an empirical solution (a function of the lateral earth pressure coefficient K) to predict the mean shear wave velocity of a soil layer, which is systematically derived in this section. Subsequently, this equation is used along with the shear wave velocity data measured by the air hammer tests to back-calculate the lateral earth pressure coefficient of the soil layers in the centrifuge.

4.1 Empirical equation to estimate v_s at a certain depth

The vertical effective stress $\sigma'_{v,m}$ at depth h_m from the soil surface in the centrifuge model is a nonlinear relationship (Taylor 1995):

$$\sigma'_{v,m} = \rho\omega^2 h_m \left(R_t + \frac{h_m}{2}\right) \quad (5)$$

where ω is the angular rotational speed of the centrifuge (equal to 183 rpm in this study) and R_t is the radius from the central axis of the centrifuge to the top of the soil model (1.505 m in this study).

Consequently, the empirical equation to estimate v_s of Congleton sand at depth h_m in the centrifuge can be obtained by manipulating Equations 4 and 5:

$$v_s = \sqrt{B\frac{(2.17-e)^2}{(1+e)\rho}\left(\rho\omega^2 h_m R_t + \rho\omega^2\frac{h_m^2}{2}\right)^{0.5}(K)^{0.25}} \quad (6)$$

where B can be obtained from bender element tests, presented below, and using e = 0.512 for the prepared soil samples in this study.

4.2 Empirical equation to calculate v_s and K of a soil layer

Equation 6 provides a method to estimate the velocity at a discrete point within a centrifuge model. However, as discussed previously, the shear wave velocity is measured over a layer with finite thickness and hence provides an average shear wave velocity. Theoretically, Equation 6 could be used to determine what the expected average shear wave velocity over a layer would be by assuming K is constant. The travel time dt within an infinitely thin soil layer dh_m is given by:

$$dt = \frac{dh_m}{v_s} \tag{7}$$

The travel time, t, within a certain soil layer with thickness, ΔH, can be obtained by integrating the above equation with respect to h_m from depth h_1 to h_2:

$$t = \int_{h_1}^{h_2} \frac{dh_m}{v_s} = \int_{h_1}^{h_2} \frac{dh_m}{\sqrt{B\,\frac{(2.17-e)^2}{(1+e)\rho}\left(\rho\omega^2 h_m R_t + \rho\omega^2 \frac{h_m^2}{2}\right)^{0.5}(K)^{0.25}}} \tag{8}$$

It should be noted that K is a parameter in Equation 8 and hence should be obtainable if the travel time within a soil layer is known. However, the integrand function in Equation 8 is a non-integrable function. Therefore, K of a certain soil layer cannot be obtained directly. Instead of solving this equation analytically, a simple method was adopted in this study to calculate K by discretizing a thick soil layer ΔH into multiple soil layers of equal thickness Δh. The shear wave velocity at the middle of each sub soil layer was taken as the mean velocity for that sub soil layer due to Δh being very small (1 mm in this study). The elapsed time within each sub soil layer Δh and the total travel time within each thick soil layer ΔH can be obtained, as well as the mean shear wave velocity. It should be noted that this method is based on the following assumptions: vertical stresses are not affected by the Duxseal and soil density is constant throughout the model. The procedure to obtain v_s of a soil layer in the centrifuge and to back-calculate K of the soil layer using air hammer test results is summarized as follows:

- Each ΔH thick soil layer (ΔH =120 mm in this study) in the centrifuge is divided into 120 sub soil layers with a thickness of Δh =1 mm.
- Shear wave velocity at the middle point $h_{m(j)}$ of each sub soil layer Δh is taken as the mean velocity $v_{s(j)}$. The travel time t_j within the sub soil layer Δh can be obtained by:

  $$t_j = \frac{\Delta h}{v_{s(j)}} \tag{9}$$

  where $v_{s(j)}$ is determined by Equation 6 and j =1, 2, 3 . . . 120.
- The travel time t within a thick soil layer ΔH can be obtained:

$$t = \sum_{j=1}^{120} t_j = \sum_{j=1}^{120} \frac{\Delta h}{v_{s(j)}} \tag{10}$$

- The theoretical mean shear wave velocity v_s within layer ΔH can be obtained by manipulating Equations 6 and 10:

$$v_s = \frac{\Delta H}{t} = \frac{\Delta H}{\Delta h} (P_1)^{0.5} (K)^{0.125} \sum_{j=1}^{120} \left(P_2 h_{m(j)}^2 + P_3 h_{m(j)} \right)^{0.25} \tag{11}$$

where $P_1 = B \frac{(2.17-e)^2}{(1+e)\rho}$, $P_2 = \frac{\rho\omega^2}{2}$ and $P_3 = \rho\omega^2 R_t$.

- Since the mean value of v_s of a certain soil layer can be expressed as a function of K, the measured mean velocity $v_{s,AHA}$ within layer ΔH from the air hammer test should equal v_s. Equation 11 can be manipulated to obtain a value for K of a soil layer in the centrifuge:

$$K = \left[\frac{v_{s,AHA} \Delta h}{\Delta H (P_1)^{0.5} \sum_{j=1}^{120} \left(P_2 h_{m(j)}^2 + P_3 h_{m(j)} \right)^{0.25}} \right]^8 \tag{12}$$

5 Signal processing

5.1 Travel time determination methods

As shown in FIG. 4, two perfect smooth artificial signals (Signal 1 and Signal 2), which are generated by an impact and detected by two transducers one after another, are used to explain three common methods used to determine the travel time between two transducers: the first arrival method, the peak-to-peak method, and the cross-correlation (xcorr) method (Karl 2005). Additionally, FIG. 4 shows the discrepancies in travel time obtained from the three methods if the wave period of Signal 1 is different from Signal 2, as detailed in Section 5.2.

The first arrival and peak-to-peak methods are based on the direct interpretation of the time histories. The characteristic points of the first arrival and peak points in the signals are identified and the time shift between signals are used to calculate the wave velocity. The cross-correlation method (an indirect method) determines the travel time between two correlated signals by performing a point-wise multiplication to determine where two signals are best aligned, i.e. Signal 1 and Signal 2 in FIG. 4. Signal 1 is shifted step by step and the point-wise multiplication is performed at each step to obtain the cross-correlation function. The time shift between two correlated signals is obtained at the maximum (or minimum if the signals are negatively correlated) of the cross-correlation function. As shown in FIG. 4, three dotted lines are used to demonstrate the time shifts obtained from the three methods: *tt1* from the first arrival method, *tt2* from the peak-to-peak method, and *tt3* from the cross-correlation method.

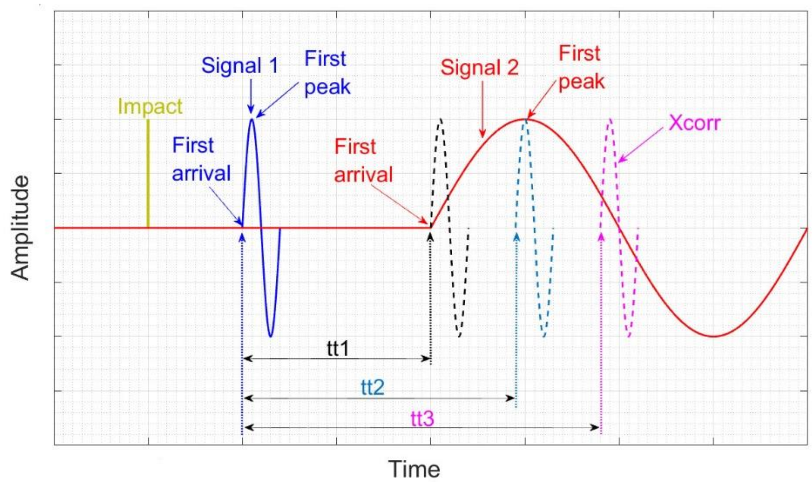

FIG. 4 Travel time analysis methods and changing wave period induced discrepancies

Typical data from the air-hammer (AHA) and bender element (BE) tests are shown in FIG. 5. Data from AHA and BE tests at all depths had a similar pattern. FIG. 5 (b) presents extracted one cycle data (see dashed boxes in FIG. 5 (a)) obtained by the four MEMS accelerometers to: a) highlight the challenge associated with collecting sufficiently high-resolution data from the air hammer tests in the centrifuge, and b) illustrate the changing wave period with depth. It should be noted that the time for each extracted signal in FIG. 5 (b) is zeroed at the first point a signal is detected. The effect of the changing wave period along depth on signal interpretation is discussed in Section 5.2. It can be seen from FIG. 5 (b) that only about 9 to 10 data points over one cycle were recorded, even with a sampling frequency of 100 kHz. In contrast, with a sampling rate of 2000 kHz, high-resolution signals were obtained from the bender element test.

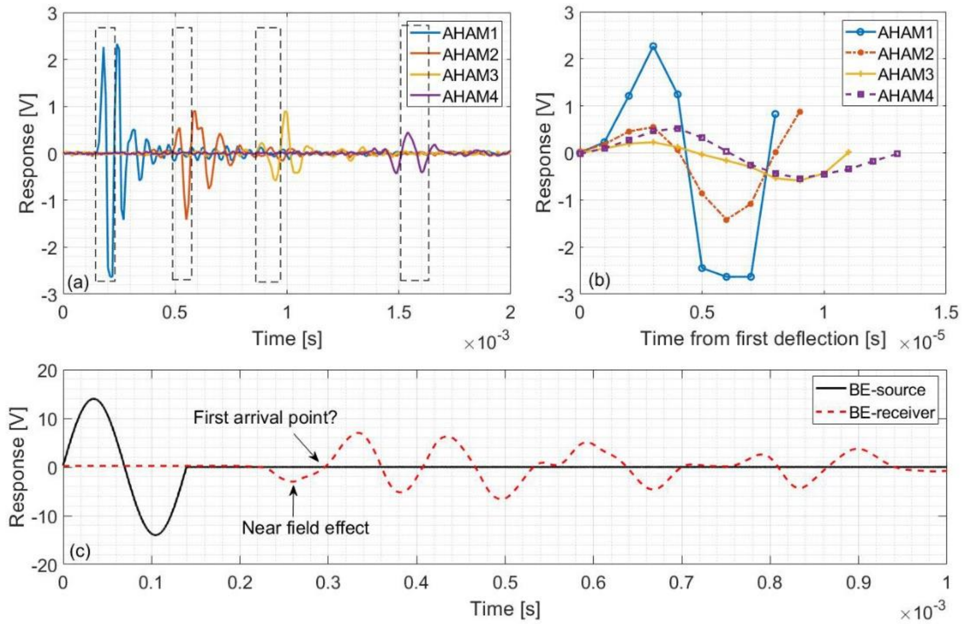

FIG. 5 (a) Typical data from an air-hammer test (b) Extracted one cycle AHA data (c) Typical data from a bender element test

A key challenge is therefore determining the travel time between two transducers accurately and consistently. Normalised shear waves measured from the air hammer tests by AHA-M1 and AHA-M4 with and without the side Duxseal are shown in FIG. 6 to: a) explain difficulties in data interpretation, and b) illustrate differences between signals with and without the side Duxseal. The two direct time methods are the most straightforward way to obtain the travel time. However, the identification of the chosen characteristic points from AHA signals is very difficult and requires some experience from the operator because measured discrete signals are usually affected by several issues: reflected waves from the rigid container boundaries, decay of the wave signals, electrical noise, and mechanical vibrations from the centrifuge. The air hammer testing related issues mentioned above can mask or distort the real first peaks and first arrival points which can lower the accuracy of the direct time methods. It can be seen from FIG. **6** (a), the first arrival and peak points of the signals from AHA-M1 are relatively easy to identify compared to the signals from AHA-M4 for which the amplitudes were relatively low. Except for AHA-M1, it can be seen from FIG. 6 (b) that it is very difficult to determine the real first arrival point and the real first peak point, with signals being distorted by the above issues. Additionally, as shown in FIG. 5 (b), about 9 to 10 data points over one cycle were recorded, and this low-resolution data can further reduce the accuracy of the peak-to-peak method, as well as the first arrival method. This is because the measured first arrival or peak points on a discrete curve may not be the real points on an analog signal. As shown in FIG. **5**, in terms of the bender element testing, the near field effect can also mask the first arrival point of the shear wave measured by the receiver, as detailed by Cui et al. (2018).

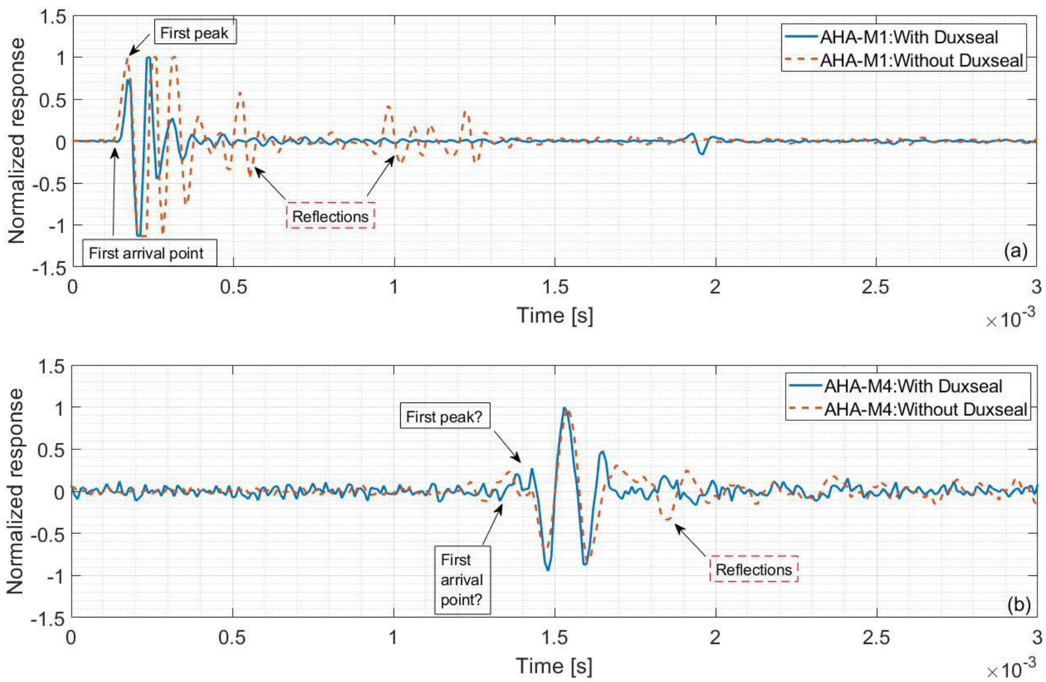

FIG. 6 Normalized AHA signals with and without side Duxseal

As explained above, the manipulation of the cross-correlation (xcorr) method avoids complications with picking characteristic points from discrete signals, hence this approach was adopted in this study to analyze detected signals from both tests. Readers may also refer to the Appendix, which demonstrates the reasoning for the adoption of the cross-correlation method in this study by comparing results obtained from these three methods.

5.2 Xcorr method: signal interpretation error

Equation 12 indicates that the evaluation of lateral earth pressure coefficient and soil stiffness profile within the centrifuge model mainly relies on a) appropriate interpretation of shear wave velocities, and b) determination of the constant B. The latter is detailed in Section 6.1, where two series of tests were performed to obtain an average value. The accuracy of the former is mainly affected by two aspects related to the proper manipulation of the cross-correlation method: data length used to perform the cross-correlation analysis, and varying wave periods, as described below.

As illustrated in FIG. 2, both shear waves and pressure waves are generated by the air hammer when the pellet impacts one end of the air hammer. These waves travel, reflect, and are recorded by the four MEMS accelerometers. FIG. 6 presents the normalized waveforms obtained from air hammer tests with and without the side Duxseal. One feature that can be observed from FIG. 6 is that the first 2 cycle waveforms are close to each other for both cases. However, after the first two cycles, the waveforms diverge. With Duxseal, waves decay quickly after the first two cycles, then slightly larger signals are recorded. However, without the side Duxseal, signal amplitudes tend to decrease first, and then much larger signals are detected after the first 2 cycles. This indicates the wave absorbing material does effectively reduce reflections, consistent with the results found by Madabhushi (1991) that Duxseal can absorb approximately 65% of incident P-waves and 60% of incident S-waves. It should be noted that the detected larger signals without the side Duxseal after the first two cycles are the distorted undesired signals and can result in inaccurate estimations from the cross-correlation method. This is because the cross-correlation method performs a point-wise multiplication to determine where two signals are best aligned, as explained previously. As discussed by Cui et al. (2018), including the data after the first cycle of the shear wave (i.e. distorted data) can result in a lower estimate of shear wave velocity by approximately 10%. Therefore, data from the first detected shear wave cycle was selected from the recorded signals and used to perform the cross-correlation analysis. Another important aspect which affects the accuracy of the cross-correlation method is the inconsistent shear wave period. It can be seen from FIG. 4 that the wave periods of Signal 1 and Signal 2, denoted as T1 and T2, are quite different (a much larger T2 is depicted in the figure to clearly show the three travel time determination methods and illustrate the error from the xcorr method caused by two wave signals with different periods). It can be seen from FIG. 5 (b) that the wave period at greater depths (AHA-M1) was smaller than at shallow depths (AHA-M4). This is because soil stiffness increases with depth, which results in the gradual decrease of shear wave period with increasing depth. The varying shear wave period with depth can lead to a travel time error, explained as follows.

As shown in FIG. 4, for the two perfect artificial sinusoidal signals, the real travel time should be the time difference between the first two arrival points even if the two signals have different periods: *tt1*. However, the travel time obtained from the xcorr method is tt3=tt1+(T2-T1)/2 and the travel time error is (T2-T1)/2. This error should be subtracted from the travel time obtained from the xcorr method; failing to do so would give shear wave velocities from the xcorr method that are smaller than the real value because the xcorr method would provide a larger travel time. This varying period effect on the estimated shear wave velocity obtained from the cross-correlation method has not been presented by previous researchers. It is therefore important to quantify this error. To obtain the shear wave period at each depth ($T_{AHA,1}$, $T_{AHA,2}$, $T_{AHA,3}$ and $T_{AHA,4}$), the first cycle of each signal was extracted from the data recorded by the air hammer MEMS accelerometers and a Fast Fourier Transform was performed. The peak values and the corresponding frequencies, $f_{AHA,1}$, $f_{AHA,2}$, $f_{AHA,3}$ and $f_{AHA,4}$, can be obtained from the frequency domain. Subsequently, the shear wave periods can be calculated, and v_s can be corrected by subtracting the error. Table 2 shows the mean wave periods and mean values of v_s obtained from over 10 air hammer test strikes in centrifuge test AHA-T2 where Duxseal was placed along the base and sides of the centrifuge container.

Table 2 Mean wave period and v_s from test AHA-T2 before and after correction

Shear wave period	Mean v_s before correction	Mean v_s after correction	Error
$T_{AHA,4}$: 12.6 × 10^{-5} s	-	-	-
$T_{AHA,3}$: 8.18× 10^{-5} s	$v_{s,AHA,3}$: 229.1 m/s	$v_{s,AHA,3}$: 237.8 m/s	3.6%
$T_{AHA,2}$: 7.78 × 10^{-5} s	$v_{s,AHA,2}$: 304.1 m/s	$v_{s,AHA,2}$: 308.8 m/s	1.5%
$T_{AHA,1}$: 6.28 × 10^{-5} s	$v_{s,AHA,1}$: 342.9 m/s	$v_{s,AHA,1}$: 350.4 m/s	2.1%

It can be seen from Table 2 that the wave period decreased with soil depth. Compared with the bottom three positions, the wave period at the uppermost depth, $T_{AHA,4}$, was much larger. The error in wave velocity resulting from the varying period was approximately 3.6% for the top soil layer. Consequently, the resulting error in G_{max} would be up to 8% for the top soil layer. This error should not be ignored and, as such, all soil stiffness related parameters from the air hammer tests presented in the following sections have had this correction applied.

6 Test results

6.1 Bender element test results: isotropic versus anisotropic

Shear wave velocities measured from isotropic and anisotropic tests and the trend of v_s with stress level were found to fit a power function in the form of Equation 4, as shown in FIG. 7. According to the curve fitting analysis, the constant *B* in Equation 4 for isotropic and anisotropic tests was 6937 and 7023, respectively. The difference is approximately 1%, which indicates that the constant *B* in Equation 4 can be assumed to be stress state independent. The value for constant *B* of dry Congleton sand adopted in subsequent analyses was taken as the average of these values, *B* = 6980.

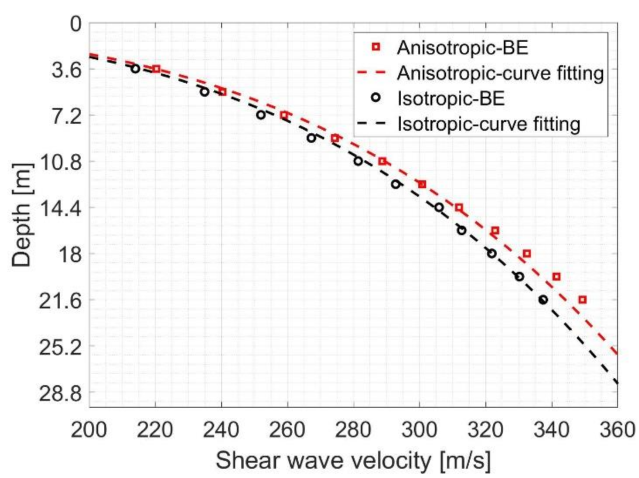

FIG. 7 Shear wave velocity: isotropic versus anisotropic (BE)

6.2 Lateral earth pressure in the centrifuge

Following the procedure detailed in Section 4, the equivalent lateral earth pressure coefficients can be calculated from Equation 12 using the air hammer test results under two conditions: with and without side Duxseal. The results are illustrated in Table 3.

TABLE 3 v_s and K in centrifuge tests with and without side Duxseal

Soil layer	Soil depth (m)	Without Duxseal		With Duxseal	
		$v_{s,AHA}$ (m/s)	K	$v_{s,AHA}$ (m/s)	K
L_3	3.6-10.8	256.7	0.52	237.8	0.28
L_2	10.8-18.0	311.8	0.52	308.8	0.48
L_1	18.0-25.2	349.4	0.53	350.4	0.54

Without Duxseal

It can be seen from Table 3 that, for the test without side Duxseal, K is relatively constant at about 0.52 within all three soil layers. The calculated value of K without Duxseal is close to the at-rest earth pressure coefficient $K_0 = 1 - sin(\varphi')$ (Jaky 1944) which, for Congleton sand with a critical state friction angle of 31° (see Table 1), gives K_0 = 0.485. Two possible reasons for the slightly higher value of K = 0.52 are that a) the soil density may have increased slightly and b) the inter-instrument spacing may have decreased slightly at 60 g compared to 1 g, which can lead to a larger measured $v_{s,AHA}$ from the air hammer tests. A 2 mm surface settlement during the spin-up of the centrifuge was measured by a displacement transducer, which leads to an average increase in soil density of 0.5%. The resulting increase in K due to density variation can be estimated by Equation 12, and it is 1% larger. The inter-instrument spacing induced increase in K is also evaluated by Equation 12 by assuming the distance between two accelerometers decreases by 0.5 mm, and the resulting increase in K is approximately 3.4%, depending on the shear wave velocity. The above two factors could increase K from 0.485 to 0.51, which is close to the measured value reported in Table 3. In general, the measured K values without Duxseal are close to the assumed at-rest earth pressure coefficient and are constant with depth. This suggests that the soil mass was in a state of elastic equilibrium and that a normally consolidated dry sand can be obtained in the centrifuge with a rigid side boundary condition.

With Duxseal

Equivalent values for the test with Duxseal placed around the inside edges of the model container are presented in Table 3, which indicates that K increases with depth. The values of K within the bottom two thirds of the soil layer are relatively close to theoretical value of K_0 = 0.48. However, K is very low, approximately 0.3, at shallow depths. According to Rankine's theory of active earth pressure (Rankine 1857), the coefficient of active earth pressure, K_a, for Congleton sand is 0.32. This suggests that the side Duxseal near the surface provided a relatively flexible boundary condition, resulting in insufficient support to the soil to maintain an 'at rest' condition. The Duxseal near the surface was likely squeezed upwards (nothing was placed on the top edge of the Duxseal to prevent this – see FIG. 2) which, assuming a nearly constant volume scenario for the Duxseal with a Poisson's ratio of 0.46 (Popescu and Prevost 1993) and very low permeability (Cilingir 2009), results in horizontal straining of the soil, mobilizing an active failure mode. It can also be seen from Table 3 that, with Duxseal along the boundary sides, the lateral earth pressure coefficient increased with depth. The lateral earth pressure coefficient of the bottom soil layer, 0.54, is close to that without side Duxseal, 0.53. This indicates that, at lower depths in the test with side Duxseal, an equivalent rigid boundary was achieved under the given test setup detailed above, and the initial K_0 condition was maintained. This would occur if, assuming constant-volume response to loading, the Duxseal at lower depths was sufficiently confined from above (by the weight of the Duxseal above it) to resist the lateral soil stress without any significant lateral straining.

These results indicate that, by confining the Duxseal near the soil surface (i.e. preventing the squeezing of Duxseal in the upwards direction), an appropriate K_0 condition could be achieved at the shallower depths. This was, however, not tested in the current study.

6.3 Duxseal effect on soil stiffness

Based on the results from the bender element tests, Equations 2 and 6 can be manipulated to obtain an equation to estimate the small strain shear modulus with depth of the dry Congleton sand in the centrifuge:

$$G_{max} = 6980\frac{(2.17-e)^2}{(1+e)}\left(\rho\omega^2 h_m R_t + \rho\omega^2\frac{h_m^2}{2}\right)^{0.5} K^{0.25} \qquad (13)$$

All parameters in Equation 13 were defined in previous sections, and the measured equivalent lateral earth pressure coefficients of the three soil layers with and without Duxseal are presented in Table 3. It should be noted that the lateral earth pressure coefficient of the soil layer from the ground surface to the depth of 3.6 m was not measured; it was assumed to be the same as the top measured soil layer. The shear modulus with and without Duxseal in the centrifuge were calculated using Equation 13 and plotted against depth in FIG. 8. It can be seen that the shear modulus of the top soil layer (1/3 the model depth from ground surface) obtained with side Duxseal is notably smaller than that without side Duxseal, by about 14%. This is a result of the significantly reduced horizontal stress at the shallow depths: a much smaller lateral earth pressure coefficient, 0.28, was used within this soil layer to estimate the shear modulus. This leads to a large jump between the first and the second soil layer, as shown in FIG. 8. Estimated shear modulus values within the middle and bottom soil layers are close for the two cases, with a difference of 3% and 0.7%, respectively.

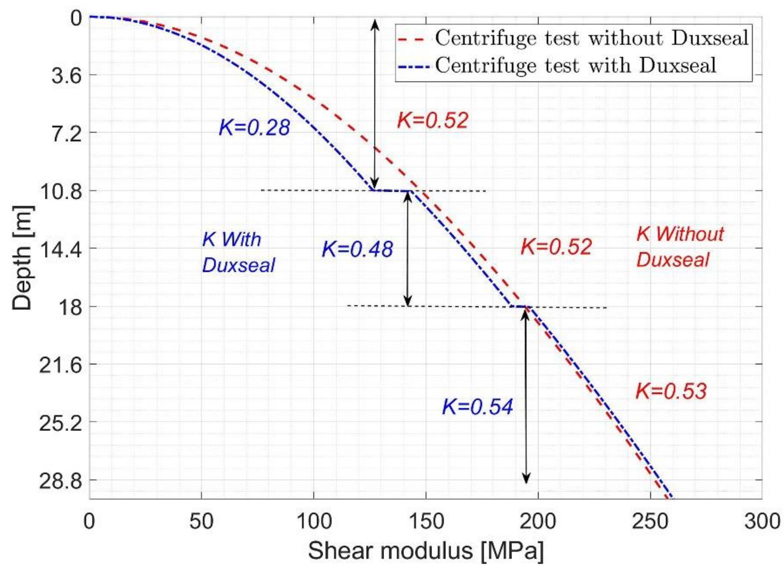

FIG. 8 Comparison of shear modulus: measurements with and without Duxseal in centrifuge

The presented results demonstrate that the initial at-rest lateral earth pressure (K_0) condition is not maintained when including Duxseal along the side boundaries of a centrifuge container. This phenomenon may alter the intended soil behavior and associated soil-structure interactions, which predominately occur within the shallower regions of centrifuge models, where it was demonstrated that Duxseal can have a significant reducing effect on small strain soil stiffness (14%). Researchers should be aware of this issue when planning centrifuge tests and when interpreting results where Duxseal is used.

6.4 Context and limitation of results

It should be noted that the proposed method is mainly relevant to small-amplitude dynamic phenomena such as ground-borne vibrations. For large-amplitude seismic studies, the outcomes of this work provides insights to potential effects, however two key features of seismic tests were not accounted for in this study, namely soil inertial effects and higher soil shear strains.

During seismic events, soil inertial effects may act to compress the energy-absorbing boundary, especially near the surface where confinement is low and the energy-absorbing material can be squeezed upwards (if not confined), thereby allowing additional lateral straining of the soil (in addition to that observed in this study) and further reducing confining stress levels within the soil. This is in contrast to this study where the soil body was essentially static with insignificant soil inertial effects.

The shear strain amplitudes in this study, about 10^{-6}, differ considerably from those in seismic events, i.e. 10^{-3}. Senetakis et al. (2013) demonstrated that a decrease in confining stress can significantly reduce the shear modulus over a wide range of shear strains, up to those applicable to seismic events, which indicates that the reductions in confining stress observed in this study would impact the large-strain shear modulus, however this study did not explicitly test under large-strain conditions. Furthermore, the combined effect of soil inertial effects and larger soil strains would need to be considered to achieve a comprehensive study applicable to seismic tests.

As such, the outcomes of this study are more applicable to future research which focuses on small ground-borne vibration events and may encourage centrifuge users to consider the potential effects of flexible boundaries for seismic centrifuge tests.

7 Conclusions and discussion

This study provided a non-intrusive approach for evaluating K_0 conditions within centrifuge models and evaluated the effect of Duxseal on the lateral stress and small strain soil stiffness in small-amplitude dynamic centrifuge models. A step-by-step procedure to obtain an empirical solution to calculate the equivalent lateral earth pressure coefficient, K, over a layer of soil in the centrifuge was presented. Details of the two types of shear wave velocity measurement tests (the bender element test in a triaxial cell and the air hammer test in the centrifuge) required to develop the empirical solution were also presented. The main conclusions are as follows.

The appropriate manipulation of the cross-correlation method used to determine the travel time is of great importance. For air hammer testing, shear waves measured from two transducers at different depths possess two different periods, thus resulting in an error using the cross-correlation method. The error increases with the difference between two periods but can be accounted for and corrected within the data processing stage.

Bender element test results under both isotropic and anisotropic stress states indicate that the constant *B*, used within an empirical methodology for predicting small strain shear modulus, is insensitive to the stress state.

The air-hammer test results indicate that, without side Duxseal, the initial at-rest lateral earth pressure (K_0) condition is satisfied. However, with side Duxseal, the lateral earth pressure coefficient K is relatively low (about 0.3) in the shallower soil region (about 1/3 the model depth from ground surface), indicating that the soil may have reached an active failure state in this region. As a result of the lateral deformation of soil, the small strain soil stiffness within the shallower soil region was estimated to have decreased by 14%. Below the top third of the model soil depth, K was found to increase and approach the K_0 condition. As a result, adopting Duxseal or other energy absorbing materials for centrifuge models will have more potential adverse consequences to applications which focus on near-surface soil behavior or shallow soil-structure interactions. These findings may also be useful for numerical modelers who should consider soil stiffness reduction to correctly validate numerical models against centrifuge test results.

It should be noted that the proposed experimental method is directly applicable to small-amplitude dynamic phenomena such as ground-borne vibrations; for large-amplitude seismic tests, the outcomes of this study provide valuable insights however the study did not account for soil inertial effects or the larger soil shear strains which are applicable to seismic tests. Further studies are required to improve the understanding of the combined effects of these factors during seismic centrifuge tests employing energy-absorbing boundaries. Despite this limitation, this study demonstrated that the effects of energy-absorbing boundaries on dynamic centrifuge models can be important, especially near the ground surface; outcomes should help researchers in prioritizing the trade-off between vibration absorbing boundaries and rigid boundaries, depending on the specific problem and the focus of their study.

References

Arulnathan, R., Boulanger, R. W., Kutter, B. L., and Sluis, W. K., 2000, "New Tool for Shear Wave Velocity Measurements in Model Tests," Geotechnical Testing Journal, Vol. 23, No. 4, pp. 444–453.

Adamidis, O., and Madabhushi, S.P.G., 2018, "Deformation mechanisms under shallow foundations on liquefiable layers of varying thickness," Géotechnique, Vol. 68, pp. 602–613.

Adamidis, O., and Madabhushi, S.P.G., 2021, "Rocking response of structures with shallow foundations on thin liquefiable layers," Géotechnique, Advance online publication. doi:10.1680/jgeot.19.P.077.

Brandenberg, S. J., Choi, S., Kutter, B. L., Wilson, D. W., and Santamarina, J. C., 2006, "A bender element system for measuring shear wave velocities in centrifuge models," 6th International Conference of Physical Modelling in Geotechnics, pp. 165-170.

BS (2005). "Mechanical vibration–Ground-borne noise and vibration arising from rail systems-Part 1: General guidance." BS ISO 148, 54.

Cilingir, U., 2009, "Seismic Response of Tunnels," Ph.D. thesis, Downing College, University of Cambridge.

Cheney, J. A., Brown, R. K., Dhat, N. R., and Hor, O. Y., 1990, "Modeling free-field conditions in centrifuge models," Journal of Geotechnical Engineering, Vol. 116, No. 9, pp. 1347–1367.

Cilingir, U., and Madabhushi, S.P.G., 2011, "A model study on the effects of input motion on the seismic behaviour of tunnels," Soil Dynamics and Earthquake Engineering, Vol. 31, pp. 452–462.

Chian, S.C., and Madabhushi, S.P.G., 2013, "Remediation against floatation of underground structures. Proceedings of the Institution of Civil Engineers," Ground Improvement, Vol. 166, pp. 155–167

Coelho, P., Haigh, S., and Madabhushi, G., 2003, "Boundary effects in dynamic centrifuge modelling of liquefaction in sand deposits," 16th ASCE Engineering Mechanics Conference.

Connolly, D. P., Kouroussis, G., Woodward, P. K., Costa, P. A., Verlinden, O., and Forde, M. C., 2014, "Field testing and analysis of high speed rail vibrations," Soil Dynamics and Earthquake Engineering, Vol. 67, pp. 102-118.

Chakrabortty, P., Popescu, R., 2012, "Numerical simulation of centrifuge tests on homogeneous and heterogeneous soil models," Computers and Geotechnics, Vol. 41, pp. 95–105.

Chian, S.C., Tokimatsu, K., Madabhushi, S.P.G., 2014, "Soil liquefaction-induced uplift of underground structures: Physical and numerical modeling," Journal of Geotechnical and Geoenvironmental Engineering, Vol. 140, doi:10.1061/(ASCE)GT.1943-5606.0001159.

Cui, G., Heron, C., and Marshall, A., 2018, "Shear wave velocity: Comparison between centrifuge and triaxial based measurements," Proceedings of the 9th International Conference of Physical Modelling in Geotechnics, Vol. 1, pp. 137–142.

Dewoolkar, M.M., Ko, H.Y., Pak, R.Y.S., 2001, "Seismic behavior of cantilever retaining walls with liquefiable backfills," Journal of Geotechnical and Geoenvironmental Engineering, Vol. 127, pp. 424–435.

Dobry, R. and Vucetic, M., 1987, "Dynamic properties and seismic response of soft clay deposits."

El-Sekelly, W., Mercado, V., Abdoun, T., Zeghal, M., and El-Ganainy, H., 2013, "Bender elements and system identification for estimation of v_s," International Journal of Physical Modelling in Geotechnics, Vol. 13, No. 4, pp. 111–121.

El-Sekelly, W., Tessari, A., and Abdoun, T., 2014, "Shear Wave Velocity Measurement in the Centrifuge Using Bender Elements," Geotechnical Testing Journal, Vol. 37, No. 4, pp. 689-704.

Ghosh, B. and Madabhushi, S. P. G., 2002, "An efficient tool for measuring shear wave velocity in the centrifuge," Proceedings of the international conference on physical modelling in geotechnics, AA

Balkema, pp. 19–124.

Ha, I.-S., Olson, S. M., Seo, M.-W., and Kim, M.-M., 2011, “Evaluation of reliquefaction resistance using shaking table tests,” Soil Dynamics and Earthquake Engineering, Vol. 31, No. 4, pp. 682- 691.

Hajialilue-Bonab, M., Chazelas, J., and Levacher, D., 2007, “Procedures used for dynamically laterally loaded pile tests in a centrifuge,” Geotechnical Testing Journal, Vol. 30, No.1, pp. 1–9.

Hardin, B. O. and Black, W. L., 1968, “Vibration modulus of normally consolidated clay,” ASCE–Proceedings – Journal of the Soil Mechanics and Foundations Division, 94(SM2, Part 1), pp. 353–369.

Hardin, B. O. and Drnevich, V. P., 1972, “Shear Modulus and Damping in Soils: Design Equations and Curves,” Journal of Soil Mechanics and Foundation Engineering Division, 98(SM7), pp. 667– 692.

Heron, C., Haigh, S., and Madabhushi, S., 2015, “A new macro-element model encapsulating the dynamic moment–rotation behaviour of raft foundations,” Géotechnique, Vol. 65, pp. 442–451.

Hughes, F.E., and Madabhushi, S.P.G., 2018, “The importance of vertical accelerations in liquefied soils,” Proceedings of the 9th International Conference of Physical Modelling in Geotechnics, doi:10.1201/9780429438646-31.

Hardin, B. O. and Richart, J. F. E., 1963, “Elastic wave velocities in granular soils,” ASCE–Proceedings–Journal of the Soil Mechanics and Foundations Division, 89 (SM1, Part 1), pp. 33–65.

Ishihara, K. (1996). Soil behaviour in earthquake geotechnics. Clarendon Press; Oxford University Press.

Itoh, K., Zeng, X., Koda, M., Murata, O., and Kusakabe, O., 2005, “Centrifuge simulation of wave propagation due to vertical vibration on shallow foundations and vibration attenuation countermeasures,” Modal Analysis, Vol. 11, No. 6, pp. 781–800.

Jaky, J., 1944, “The Coefficient of Earth Pressure at Rest,” Journal for Society of Hungarian Architects and Engineers, pp. 355–358.

Karl, L., 2005, “Dynamic soil properties out of SCPT and bender element tests with emphasis on material damping,” Ph.D. thesis, Department of Civil engineering, Ghent University.

Kassas, K., Adamidis, O., Gerolymos, N., and Anastasopoulos, I., 2020, “Numerical modelling of a structure with shallow strip foundation during earthquake-induced liquefaction,” Géotechnique.

Kassas, K., Adamidis, O., and Anastasopoulos, I., 2021, “Shallow strip foundations subjected to earthquake-induced soil liquefaction: Validation, modelling uncertainties, and boundary effects,” Soil Dynamics and Earthquake Engineering, Vol. 147.

Kim, N. R., Kim, D. S., 2010, “Development of Vs tomography testing system for geotechnical centrifuge experiments,” 7th International Conference of Physical Modelling in Geotechnics, Springman, Vol. 50, No. 1, pp. 349–354.

Kouroussis, G., Connolly, D. P., and Verlinden, O., 2014, “Railway-induced ground vibrations-a review of vehicle effects,” International Journal of Rail Transportation, Vol. 2, No. 2, pp. 69-110.

Lauder, K., 2010, “The performance of pipeline ploughs,” Ph.D. thesis, Department of Civil Engineering, University of Dundee.

Lee, C.-J., Hung, W.-Y., Tsai, C.-H., Chen, T., Tu, Y., and Huang, C.-C., 2014, “Shear wave velocity measurements and soil–pile system identifications in dynamic centrifuge tests,” Bulletin of earthquake engineering, Vol. 12, No. 2, pp. 717–734.

Lee, C.-J., Wang, C.-R., Wei, Y.-C., and Hung, W.-Y., 2012, “Evolution of the shear wave velocity during shaking modeled in centrifuge shaking table tests,” Bulletin of earthquake engineering, Vol. 10, No. 2, pp. 401–420.

Lee, J.-s. and Santamarina, J. C., 2005, “Bender Elements: Performance and Signal Interpretation,” Journal of Geotechnical and Geoenvironmental Engineering, Vol. 131, No. 9, pp. 1063–1070.

Lombaert, G., Degrande, G., François, S., and Thompson, D. J., 2015, “Ground-Borne Vibration due to Railway Traffic: A Review of Excitation Mechanisms, Prediction Methods and Mitigation Measures,” Noise and Vibration Mitigation for Rail Transportation Systems: Proceedings of the 11th International Workshop on Railway Noise, Vol. 126, pp. 253–287.

Madabhushi, G., 1991, “Response of tower structures to earthquake perturbations,” Ph.D. thesis, University of Cambridge.

Madabhushi, S.S.C., and Haigh, S.K., 2019, “Using tactile pressure sensors to measure dynamic earth pressures around dual-row walls,” International Journal of Physical Modelling in Geotechnics, Vol. 19, pp. 58–71.

Madabhushi, S.S.C., and Haigh, S.K., 2021, "On the dynamic response of flexible dual-row retaining walls in dry sand," Géotechnique, Advance online publication. doi:10.1680/jgeot.19.P.189.

Mitaritonna, G., Amorosi, A., and Cotecchia, F., 2010, "Multidirectional bender element measurements in the triaxial cell: equipment set-up and signal interpretation," Italian Geotechnical Journal, pp. 51-69.

Kumar, J., and Madhusudhan, B.N., 2010, "Effect of relative density and confining pressure on Poisson ratio from bender and extender elements tests," Géotechnique, Vol. 60, No. 7, pp. 561-567.

Pak, R. Y. S. and Guzina, B. B., 1995, "Dynamic characterization of vertically loaded foundations on granular soils," Journal of geotechnical engineering, Vol. 121, No. 3, pp. 274–286.

Popescu, R., and Prevost, J.H., 1993. "Centrifuge validation of a numerical model for dynamic soil liquefaction," Soil Dynamics and Earthquake Engineering, Vol. 12, No. 2, pp. 73–90.

Pak, R.Y., Soudkhah, M., and Abedzadeh, F., 2011, "Experimental synthesis of seismic horizontal free-field motion of soil in finite-domain simulations with absorbing boundary," Soil Dynamics and Earthquake Engineering, Vol. 31, pp. 1529-1539.

Rankine, W., 1857, "On stability of Loose Earth. Philosophic Transactions of Royal Society," London.

Rollins, K. M., Evans, M. D., Diehl, N. B., and Daily III, W. D., 1998, "Shear modulus and damping relationships for gravels," Journal of Geotechnical and Geoenvironmental Engineering, Vol. 124, No. 5, pp. 396–405.

Senetakis, K., Anastasiadis, A., and Pitilakis, K., 2013, "Normalized shear modulus reduction and damping ratio curves of quartz sand and rhyolitic crushed rock," Soils and Foundations, Vol. 53, pp. 879–893. doi: https://doi.org/10.1016/j.sandf.2013.10.007.

Stokoe, K., Lee, S., and Knox, D., 1985, "Shear moduli measurements under true triaxial stresses," Advances in the art of testing soils under cyclic conditions, ASCE, pp. 166–185.

Soudkhah, M., and Pak, R.Y., 2012, "Wave absorbing-boundary method in seismic centrifuge simulation of vertical free-field ground motion," Computers and Geotechnics, Vol. 43, pp. 155–164.Taylor, R. N., 1995, "Geotechnical Centrifuge Technology," Blackie Academic and Professional, London.

Thusyanthan, N. I. and Madabhushi, S. P. G., 2003, "Experimental study of vibrations in underground structures," Proceedings of the Institution of Civil Engineers: Geotechnical Engineering, Vol. 156, No. 2, pp. 75–81.

Yang, W., 2012, "Physical and numerical modelling of railway induced ground-borne vibration," Ph.D. thesis, Department of Civil Engineering, University of Nottingham.

Yang, W., Hussein, M.F.M. and Marshall, A., 2013a, "Centrifuge and numerical modelling of ground-borne vibration from an underground tunnel," Soil Dynamics and Earthquake Engineering, Vol. 51, pp. 23-34.

Yang, W., Hussein, M. F. M., Marshall, A. M., & Cox, C., 2013b, "Centrifuge and numerical modelling of ground-borne vibration from surface sources". Soil Dynamics and Earthquake Engineering, 44, 78–89.

Zeng, X. and Schofield, A. N., 1996, "Design and performance of an equivalent-shear-beam container for earthquake centrifuge modelling," Géotechnique, Vol. 46, No. 1, pp. 83–102.

Zhu, B., Li, J., Wang, L., and Chen, Y., 2018, "Centrifugal model tests on static and seismic stability of landfills with high water level," Proceedings of the 9th International Conference of Physical Modelling in Geotechnics.

Appendix A

Comparison of shear wave velocity determination methods

Shear wave velocities and the corresponding lateral earth pressure coefficients obtained using the first arrival, peak-to-peak, and cross-correlation (Xcorr) methods with and without Duxseal are illustrated in the tables below. Note that, as discussed in Section 6.2, an at-rest earth pressure coefficient K_0 between 0.49 and 0.51 is expected. Table A.2 presents data for no Duxseal and shows that most of the lateral earth pressure coefficients obtained from all methods are close to the expected values at the deepest location. In addition, the cross-correlation method is shown to give consistent results at all depths (which is expected for this test), whereas the first arrival and peak-to-peak methods show considerable variability and unrealistically/unexpectedly high and low values of K_0, for example 0.44 and 0.73. This difference in consistency between the methods, with depth into the soil layer, is due to the higher signal-noise ratio obtained for the deeper locations, and hence the ease with which the different methods can determine the travel time. These results lead to the conclusion that the first arrival and peak to peak methods were acceptable, but not as suitable/reliable for the data obtained from the centrifuge-based air hammer tests.

Table A.2 shows the equivalent data for tests including Duxseal and illustrates that the lateral earth pressure coefficient obtained from all methods is relatively low near the surface and increases with depth. The first arrival and peak-to-peak results agree reasonably well with the cross-correlation method, however, due to the variability of these test results illustrated in Table A.1, the cross-correlation results were deemed to be more reliable for this study.

TABLE A.1 v_s and K in centrifuge tests without side Duxseal

Soil layer	Soil depth (m)	First arrival		Peak to peak		Xcorr	
		$v_{s,AHA}$ (m/s)	K	$v_{s,AHA}$ (m/s)	K	$v_{s,AHA}$ (m/s)	K
L_3	3.6-10.8	253.7	0.44	260.8	0.55	256.7	0.52
L_2	10.8-18.0	315.8	0.58	325.1	0.73	311.8	0.52
L_1	18.0-25.2	343.3	0.50	342.8	0.49	349.4	0.53

TABLE A.2 v_s and K in centrifuge tests with side Duxseal

Soil layer	Soil depth (m)	First arrival		Peak to peak		Xcorr	
		$v_{s,AHA}$ (m/s)	K	$v_{s,AHA}$ (m/s)	K	$v_{s,AHA}$ (m/s)	K
L_3	3.6-10.8	234.7	0.24	235.3	0.24	237.8	0.28
L_2	10.8-18.0	307.8	0.47	315.6	0.57	308.8	0.48
L_1	18.0-25.2	347.8	0.53	353.1	0.62	350.4	0.54